Draft for *Geophys. J. Int.*

Linking elastic and electrical properties of rocks using cross-property DEM

P. A. Cilli[1,2,3*], M. Chapman[1,2]

[1] *Grant Institute, School of GeoSciences, The University of Edinburgh, James Hutton Rd, King's Buildings, Edinburgh, EH9 3FE, UK*

[2] *International Centre for Carbonate Reservoirs, Edinburgh, UK*

[3] *Current address: Department of Earth Sciences, University of Oxford, South Parks Road, Oxford, OX1 3AN, UK*

[*] *Corresponding author: Phillip.Cilli@earth.ox.ac.uk*

SUMMARY

Combining electrical and elastic measurements can be instrumental in lowering the uncertainty of subsurface characterisation. Many commonly used rock physics relations for joint electrical-elastic properties are at least partly empirical, and often rely on the estimation of porosity as an intermediate step. We combine differential effective medium schemes which relate respectively elastic and electrical properties to porosity and pore shape. The resulting expressions are independent of porosity, depending only on pore aspect ratio. Analysis of published joint electrical-elastic data shows that a single aspect ratio model performs well for clean sandstones, allowing us to model V_p/V_s ratios as a function of resistivity. Clay-bearing sandstones are more complex, but our modelling can still identify the correct trends. We speculate about the potential to extend our approach to produce additional cross-property relations.

Key words: Elasticity and anelasticity – Electrical properties – Controlled source electromagnetics (CSEM) – Joint inversion – Non-linear differential equations – Permeability and porosity

1 INTRODUCTION

Electrical-elastic multiphysics modelling, for example through the integration of controlled-source electromagnetic (CSEM) data into marine seismic reservoir characterisation workflows, can lead to reduced uncertainty in reservoir characterisation (Alcocer et al. 2013). However, a simple, physics-based, and accurate multiphysics model which links a porous rock's electrical and elastic properties remains elusive. Many existing electrical-elastic relationships are at least partly empirical (Carcione et al. 2007). In addition to this, the majority of workflows which relate a rock's elastic and electrical properties require the estimation of porosity as an intermediate step (e.g., Sevostianov & Kachanov (2002); Carcione et al. (2007); Engelmark (2010); Werthmüller et al. (2013)), which can be uncertain away from well control.

Carcione et al. (2007) presented a set of electrical-elastic cross-property models with no explicit porosity terms by substituting pre-existing resistivity-porosity models into pre-existing velocity-porosity models; a method originally used by Sevostianov & Kachanov (2002), and more recently by Han (2018), who modelled anisotropic electrical-elastic measurements made on artificial porous sandstones with aligned fractures. Chen & Dickens (2009) and Werthmüller et al. (2013) assessed the intrinsic (theoretical) and extrinsic (parametrisation) uncertainties related to the models of Carcione et al. (2007), which were generally found to be significant. In fact, Kwon & Snieder (2011) showed the uncertainty in these multiphysics models had a larger contribution to overall uncertainty than that associated with the data. Electrical-elastic cross-property bounds exists which have no explicit porosity terms and are derived from first principles, such as the Hashin-Shtrikman bounds (Carcione et al. 2007), but these can be too widely spaced to predict the physical properties of any rock in particular.

Estimating the Earth's shear modulus is an important aspect of geophysics at many scales, from understanding the composition of the Earth's mantle (Kennett et al. 1998), to estimating reservoir fluids using V_p/V_s ratios (Hamada 2004), to geotechnical soil studies (Hussien & Karray 2015). Estimating a rock's shear modulus from its electrical resistivity, however, is scarcely addressed in the geophysical literature, and has been done predominantly using empirical methods (Jones et al. 2013; Yasir et al. 2018). The problem of modelling a rock's shear modulus and hence V_p/V_s ratio from electrical resistivity measurements alone by a simple model derived from first principles remains unsolved.

Joint electrical-elastic modelling with a single model parameter has been attempted with mixed success (Han et al. 2011a; Wang & Gelius 2010; Jensen et al. 2013). Notwithstanding, a scrutiny by Han et al. (2016) concluded a new multiphysics model was required to accurately relate the electrical and elastic properties of a porous rock using a single set of model parameters. Werthmüller et al. (2013) note that there is no known direct link between a rock's velocity and resistivity.

Recently, Han et al. (2020) experimentally determined the relationship between a clean sand-

stone's pore shape and grain shape parameters, which are used in elastic and electrical differential effective medium (DEM) models respectively when modelling independently the elastic and electrical properties of rocks. In doing this, Han et al. (2020) answered the outstanding question of whether there was some unknown pore-to-grain shape correlation which would enable existing DEM models to become suitable for joint electrical-elastic modelling. Thus it was shown that standard DEM models can be used for cross-property modelling, however the method relies upon an empirical, laboratory-derived relation. It currently seems the standard DEM models do not allow for cross-property modelling without incorporating empirical relations in some way, and so their reformulation may be necessary to derive a cross-property DEM model from first principles.

In this paper, we present a new functional form of a DEM model which relates the electrical and elastic properties of an isotropic, porous rock. The model is derived using the technique of Sevostianov & Kachanov (2002) and Carcione et al. (2007), where an electrical model is substituted into an elastic model through the common independent variable, porosity. The theoretical advantage of the proposed model on existing models is that it is derived from first principles, has no porosity terms, is correct in the high and low porosity asymptotes, has a single, intuitive parameter, and can be expressed in terms of the geometrical functions $Q^{(*2)}$, $P^{(*2)}$, and $R^{(*2)}$, proposed by Berryman (1980, 1995).

We test the forward and inverse model on the wet, mixed sandstone core measurements of Han et al. (2011b) and show both are accurate in the case of clean sandstones and less accurate in the presence of clay for this data set. We also show the single model parameter, equivalent pore aspect ratio, is weakly sensitive to clay volume fraction in this data set. In addition to this, we demonstrate that one can model a V_p/V_s trend for this collection of mixed, wet sandstones using only electrical conductivity measurements and an empirical velocity-density relation once the model is parameterised, with accuracy comparable to the V_p/V_s model of Han et al. (1986).

To begin, we reformulate the electrical differential effective medium (DEM) model of Mendelson & Cohen (1982) for the case when ellipsoidal fluid-filled pores are embedded in a background of mineral matrix, contrasting with the typical expression which embeds grains into a background of water. Following this, we combine this electrical DEM expression with the analogous elastic DEM expressions of Berryman (1992) using the technique of Sevostianov & Kachanov (2002) and Carcione et al. (2007) for cross-property modelling - which in the case of DEM equates to applying the chain rule - to obtain new electrical-elastic DEM expressions which predict elastic moduli from electrical conductivity measurements. We then test this cross-property DEM model's performance on the laboratory electrical-elastic measurements of Han et al. (2011b), which are made on brine-flooded sandstone cores from multiple localities, having a range of clay and pore volume fractions. We estimate the optimal parameters which model the rock's bulk and shear modulus, and investigate the effect of clay

content on the model's parametrisation and uncertainty. Following this, we predict a V_p/V_s trend for mixed, wet sandstones in the absence of porosity and density measurements using the modelled elastic moduli and the Gardner et al. (1974) velocity-density relation for sandstones. Finally, we solve the inverse problem numerically to estimate electrical resistivity from measured elastic moduli and assess the effect of clay content on the inverse solution.

2 MODEL DERIVATION

2.1 Electrical modelling

Electrical inclusion modelling was first popularised by Maxwell Garnett (1904), who proposed an effective medium approximation to calculate the electrical properties of a material containing spherical inclusions. This was followed by Bruggeman (1935), who proposed an electrical DEM model for the same material. By devising a DEM model which embedded fractal-layered insulating spherical grains into a background initially made of water, Sen et al. (1981) derived Archie's (Archie 1942) first law with cementation exponent $m = 1.5$ and tortuosity $a = 1$.

Recognising it is unrealistic to approximate pores, grains, and inclusions in general with spheres, ellipsoidal inclusions became favoured when analytically modelling the electrical properties of composite materials due to their ability to approximate reality more accurately while still producing analytically tractable models. Polder & Van Santeen (1946) estimated the average electrical properties of an isotropic medium containing randomly oriented ellipsoidal inclusions which are assumed to be non-interacting, before Frank (1963) calculated the effective electric field in a medium containing a single homogeneous ellipsoid with principal axes arbitrarily aligned with respect to the incident electric field. Extending the work of Sen et al. (1981), Mendelson & Cohen (1982) developed a DEM model to calculate the effective electrical properties of a medium containing many arbitrarily oriented ellipsoidal inclusions in a uniform, static electric field.

Arguably the most renowned aspect of the DEM model of Mendelson & Cohen (1982), abbreviated to "M&C" henceforth, is a subsidiary result: by setting the grain conductivity to zero, fluid conductivity to that of water, and letting ellipsoidal grains be randomly oriented, M&C's electrical DEM model takes the form of Archie's (Archie 1942) first law:

$$\sigma^* = \sigma_w \phi^m \,. \tag{1}$$

Parameter σ^* is the rock's overall conductivity, σ_w is the saturating water's conductivity, and m is the cementation factor. We note tortuosity factor a, a common coefficient of Archie's first law (Glover 2016), can be said to be unity in equation 1, as is also derived in the electrical DEM model of Sen

et al. (1981) for spherical grains. Importantly, M&C showed m is a function of grain aspect ratio α, agreeing with observations that m depends on grain shape (e.g., Salem & Chilingarian (1999)).

M&C consider a rock with background material volume fraction (porosity) ϕ, background material conductivity σ_2, and inclusion (i.e., grain) conductivity σ_1. M&C's DEM model in its most general form for inclusions of a single aspect ratio is then:

$$d\sigma^* = -\frac{d\phi}{\phi}\left\langle (\sigma_1 - \sigma^*)\left[1 + (\sigma^*)^{-\frac{1}{2}}\,\boldsymbol{\Theta}_1\,(\sigma^*)^{-\frac{1}{2}}\,(\sigma_1 - \sigma^*)\right]^{-1}\right\rangle ; \tag{2}$$

where angled brackets denote an average over all inclusion orientations and $\boldsymbol{\Theta}_1$ is a 3×3 matrix, such that:

$$\boldsymbol{\Theta}_1 = \mathbf{R}\mathbf{L}\mathbf{R}^{-1} . \tag{3}$$

Matrix $\boldsymbol{\Theta}_1$ (Frank 1963) contains the effective depolarisation factors of an ellipsoidal inclusion of phase 1 which is arbitrarily rotated with respect to an incident electric field. Matrix $\mathbf{L}$ is the diagonal matrix with the ellipsoid's three depolarisation factors L_p, $p \in \{1, 2, 3\}$, along its diagonal. Depolarisation factors L_p (e.g., Osborn (1945)) are the shape-dependent scalars which map from the scalar component of an external electric field applied along the ellipsoid's p^{th} axis, $\mathscr{E}_p$, to the ellipsoid's dipole moment along its p^{th} axis, $\mathscr{P}_p$, through the relation:

$$\mathscr{P}_p = \frac{\mathscr{E}_p V}{4\pi L_p} , \tag{4}$$

where V is the ellipsoid's volume. Matrix $\mathbf{L}$ has trace unity, and $\mathbf{R}$ is an orthogonal matrix. In the case of randomly oriented ellipsoidal grains, $\mathbf{R} = \mathbf{I}$ and the rock's effective conductivity is isotropic, presuming an isotropic background conductivity. In this paper, we only consider the isotropic case and so set $\boldsymbol{\Theta}_1 = \mathbf{L}$ henceforth.

To derive equation 1, M&C make the approximation that grains are perfect resistors by setting $\sigma_1 = 0$ in equation 2 and obtain the differential equation:

$$\frac{d\sigma^*}{\sigma^*} = m\frac{d\phi}{\phi} ; \tag{5}$$

with cementation factor m:

$$m = \frac{1}{3}\sum_{p=1}^{3}\left\langle [1 - L_p]^{-1}\right\rangle . \tag{6}$$

Taking the average of equation 6 over all grain orientations and integrating with the boundary condition $\sigma^*\,(\phi = 1) = \sigma_2$ yields equation 1 with $\sigma_2 = \sigma_w$.

Our current aim is to reformulate the DEM model of equations 5 and 6 with reversed phases, embedding fluid-filled pores into a background of matrix material. To do this, we change the variable ϕ to $(1-\phi)$ and interchange subscripts 1 and 2 in equation 2 to obtain:

$$\frac{d\sigma^*}{\sigma^* - \sigma_2} = \bar{m}\frac{d\,(1-\phi)}{(1-\phi)}\,; \tag{7}$$

where we define $\bar{m}$ as:

$$\bar{m} = \frac{1}{3}\sum_{p=1}^{3}\left\langle \left[1 + \left(\frac{\sigma_2}{\sigma^*} - 1\right) L_p\right]^{-1} \right\rangle\,. \tag{8}$$

Equations 7 and 8 are a reformulation of equations 5 and 6 respectively, here with pores embedded into a background of matrix material.

Changing the independent variable in equation 7, we obtain the reformulation of M&C's electrical DEM model with ellipsoidal pores embedded into a background of matrix material, which takes the form presented by Torquato & Haslach Jr (2002):

$$\frac{d\sigma^*}{d\phi} = \frac{(\sigma_2 - \sigma^*)\,\bar{m}}{(1-\phi)}\,. \tag{9}$$

By considering spheroidal inclusions, we drop the subscript p in depolarisation factors L_p, calling the principal depolarisation factor L, and the two degenerate factors $(1-L)/2$, as the trace of $\mathbf{L}$ is unity.

Parameter $\bar{m}$ from equation 8 for randomly oriented spheroidal inclusions is thus:

$$\bar{m} = \frac{1}{3}\sigma^*\left[\frac{4}{\sigma^* + \sigma_2 + L\,(\sigma^* - \sigma_2)} + \frac{1}{\sigma^* - L\,(\sigma^* - \sigma_2)}\right]\,; \tag{10}$$

Berryman (1995) proposed a geometrical function $R^{(*2)}$ which accounts for the effect of the aspect ratio of randomly oriented spheroidal inclusions on the effective electrical conductivity in the Clausius-Mossotti and self-consistent approximations. Function $R^{(*2)}$ is defined as:

$$R^{(*2)} = \frac{1}{9}\left[\frac{4}{\sigma^* + \sigma_2 + L\,(\sigma^* - \sigma_2)} + \frac{1}{\sigma^* - L\,(\sigma^* - \sigma_2)}\right]\,; \tag{11}$$

$$= \frac{\bar{m}}{3\sigma^*}\,, \tag{12}$$

Where the superscript $(*2)$ in $R^{(*2)}$ indicates the effective and inclusion properties are used for its evaluation. Thus, by equations 9 and 12, the DEM model of M&C can now be expressed in terms of the geometric function $R^{(*2)}$:

$$\frac{d\sigma^*}{d\phi} = 3\sigma^* \frac{(\sigma_2 - \sigma^*)\, R^{(*2)}}{(1-\phi)}\,. \tag{13}$$

As an aside, we note the two-phase self-consistent electrical model for spheroidal pores of Berryman (1995) can be formulated in terms of $\bar{m}$:

$$\frac{\phi\,(\sigma_2 - \sigma^*)\,\bar{m}}{3\sigma^*} = 0\,. \tag{14}$$

This may be of interest if a physically meaningful link between $\bar{m}$ and a rock's petrophysical properties is found, as exists with the analogous m (e.g., Salem & Chilingarian (1999)) but is not so obvious with the SCA model's typical geometrical function $R^{(*2)}$.

We also see equation 9 reduces to the electrical DEM model of Bruggeman (1935) in the special case when $L = 1/3$. This result is expected as the model of Mendelson & Cohen (1982) is consistent with that of Sen et al. (1981) in the case of spherical inclusions, which in turn is consistent with that of Bruggeman (1935).

We only require equation 9 to obtain our proposed, joint electrical-elastic DEM expressions. For completeness, however, we integrate equation 9 here to obtain an expression analogous to Archie's first law as derived by M&C. For simplicity, we make the approximation that $\bar{m}$ in equation 10 is constant in σ^* by assuming $\sigma^* \ll \sigma_2$, as is often the case in rocks with fluid-filled pores. However, equation 9 can be integrated analytically with σ^*-dependent $\bar{m}$ as defined in equation 10 if desired. Integrating equation 9 with boundary condition $\sigma^*(\phi = 0) = \sigma_1$, we find the analogous equation to M&C's expression of Archie's first law:

$$\frac{\sigma_2 - \sigma^*}{\sigma_2 - \sigma_1} = (1-\phi)^{\bar{m}}\,. \tag{15}$$

2.2 Elastic modelling

Berryman (1992) presented a DEM model which estimates the effective elastic moduli of a dilute dispersion of randomly oriented ellipsoidal inclusions in an isotropic background material by the coupled equations:

$$\frac{dK^*}{d\phi} = \frac{(K_2 - K^*)\, P^{(*2)}}{(1-\phi)}\,; \tag{16}$$

$$\frac{d\mu^*}{d\phi} = \frac{(\mu_2 - \mu^*)\, Q^{(*2)}}{(1-\phi)}\,; \tag{17}$$

where K and μ denote bulk and shear moduli respectively and ϕ represents inclusion volume fraction. Sub- and superscripts 1 and 2 represent background and inclusion phases respectively, while

$*$ denotes the effective properties of the composite. Functions $P^{(*2)}$ and $Q^{(*2)}$ are defined explicitly by Berryman (1980) for the arbitrary spheroidal inclusion. The form of these functions follows from the solution of Eshelby (1957) for the deformation of an elastic ellipsoidal inclusion in a matrix under stress. In the differential effective medium approximation, functions $P^{(*2)}$ and $Q^{(*2)}$ depend on the effective moduli, the inclusion moduli, and the inclusion aspect ratio α. Analogous to the boundary condition of equation 7, equations 16 and 17 are solved with boundary conditions $K^*(\phi = 0) = K_1$ and $\mu^*(\phi = 0) = \mu_1$.

2.3 Electrical-elastic modelling using cross-property DEM

Dividing equations 16 and 17 by equation 9 - that is, employing the chain rule - we obtain a set of coupled differential equations which relate the electrical and elastic properties of a two-phase, isotropic, linearly elastic, electrically conductive composite:

$$\frac{dK^*}{d\sigma^*} = \left(\frac{K_2 - K^*}{\sigma_2 - \sigma^*}\right)\frac{P^{(*2)}}{\bar{m}}\,; \tag{18}$$

$$\frac{d\mu^*}{d\sigma^*} = \left(\frac{\mu_2 - \mu^*}{\sigma_2 - \sigma^*}\right)\frac{Q^{(*2)}}{\bar{m}}\,. \tag{19}$$

Porosity is rendered a dummy variable when the chain rule is applied, meaning equations 18 and 19 contain no porosity terms.

By equation 12, equations 18 and 19 can be expressed in terms of $P^{(*2)}$, $Q^{(*2)}$, and $R^{(*2)}$:

$$\frac{dK^*}{d\sigma^*} = \frac{1}{3\sigma^*}\left(\frac{K_2 - K^*}{\sigma_2 - \sigma^*}\right)\frac{P^{(*2)}}{R^{(*2)}}\,; \tag{20}$$

$$\frac{d\mu^*}{d\sigma^*} = \frac{1}{3\sigma^*}\left(\frac{\mu_2 - \mu^*}{\sigma_2 - \sigma^*}\right)\frac{Q^{(*2)}}{R^{(*2)}}\,. \tag{21}$$

The boundary conditions of equations 18 and 19, or 20 and 21, are:

$$K^*\left(\sigma^* = \sigma_1\right) = K_1\,; \tag{22}$$

$$\mu^*\left(\sigma^* = \sigma_1\right) = \mu_1\,. \tag{23}$$

The key conceptual difference between these cross-property DEM expressions and a typical electrical or elastic DEM model is that in the cross-property method, the porosity added in each rock-building iteration is not $d\phi$, but the unknown pore volume fraction which increments the rock's effective conductivity by $d\sigma^*$. These cross-property DEM expressions are correct in both the high and low porosity limit even though porosity is rendered a dummy variable.

Table 1. Additional physical properties also modelled by DEM through mathematical equivalency, adapted from Choy (2016).

Problem	Potential, V	$-\nabla V$	Observable	Flux density
Electrostatics	Electric potential	Electric field	Permittivity	Electric displacement
Magnetostatics	Magnetic potential	Magnetic field	Permeability	Magnetic induction
Heat conduction	Temperature	Temperature gradient	Heat conductivity	Heat flux
Diffusion	Density	Density gradient	Diffusion constant	Particle current density

2.4 Generalised cross-property DEM

The Laplace equation governs the elastic and electric fields with a low frequency source located at infinity, as is the assumption of typical inclusion models (Choy 2016) such as DEM. The universality of the Laplace equation suggests other physical properties can be modelled by DEM with mathematical equivalence; namely, thermal conductivity, electrical permittivity, magnetic permeability, and diffusion constant. Table 1, adapted from Choy (2016), presents the additional physical properties which can be modelled with mathematical equivalence to the electrical conductivity inclusion problem. It follows from this equivalence that modelling using cross-property DEM also theoretically extends to any combination of two properties from Table 1, as well as a rock's elastic moduli and electrical conductivity.

3 LABORATORY DATA MODELLING

3.1 Elastic Moduli Modelling

To test the proposed electrical-elastic DEM model, we use the laboratory data set of Han et al. (2011b). This data set is comprised of simultaneous electrical and elastic laboratory measurements made on 63 sandstone cores collected from the UK and China. At least eight minerals are present in the cores, including quartz, four clay minerals, two feldspar minerals, and carbonates. The experiments were conducted by Han et al. (2011b) with a saturating brine concentration of 35 g/L and a pore fluid pressure of 5 MPa. The electrical resistivity ($1/\sigma$) measurements had a low-frequency (2 Hz) source, as is of interest in Controlled Source Electromagnetism (CSEM) studies. Core porosity was measured by helium porosimetry, and mineralogy was determined by whole rock X-ray diffraction. The samples were maintained at 19 ± 1 degree Celsius throughout experiments. Brine-saturated compressional and shear wave velocities were measured at 1.0 MHz and 0.7 MHz respectively.

Velocities were measured at various effective pressures, ranging from 8-60 MPa (Han et al. 2011b). We study the measurements made at 60 MPa in this paper. At relatively low pressures, microcracks are more likely to be present in these samples when compared to higher pressures. The presence of

Table 2. Physical parameters used in electrical-elastic modelling.

Constituent	K (GPa)	μ (GPa)	σ $(1/(\Omega\text{m}))$	Moduli source	Conductivity source
Quartz	36.6	45.5	10^{-5}	Mavko et al. (2020)	Han et al. (2011a)
Brine	2.29	0	$1/0.213$	Han et al. (2011a)	Han et al. (2011a)

these microcracks would increase the rock's equivalent inclusion eccentricity when compared to a rock at higher pressure. Open microcracks may also allow for squirt flow over a certain frequency band (Mavko & Jizba 1991; Dvorkin & Nur 1993; Chapman et al. 2002). However, these factors are not of concern in this study as all measurements analysed are made at constant pressure and frequency.

We study only measurements from the subset of 30 cores which have quartz content greater than 60% volume fraction. We refer to this subset of measurements as the "Han" data henceforth. By considering only these measurements, we ensure mineralogy is quartz-dominated. Accordingly, we model all data assuming samples have a pure quartz matrix. The clay volume fraction is non-negligible in many samples, as is shown in Figure 1. By modelling the properties of clay-bearing rocks with the assumption of pure quartz matrix, we can test the impact of clay content on the model's parametrisation. All electrical and elastic parameters used in modelling are shown in Table 2.

To investigate the effects of clay on the electrical-elastic model, we partitioned the Han data into clean and clay-bearing data by arbitrarily choosing a threshold of 3.5% clay volume fraction, as shown in Figure 1. This is of interest as the electrical properties of a rock are affected by the presence of clay through the double layer effect (Waxman & Smits 1968), which the proposed electrical-elastic model does not account for. In addition to this, the elastic moduli of a sandstone can also be significantly affected by only a small amount of clay (Han et al. 1986).

We refer to the model's parameter α as the equivalent pore aspect ratio (EPAR) when applied to real data, following Fournier et al. (2011, 2014, 2018) and Cilli & Chapman (2020). We differentiate between "EPAR" in applied inclusion modelling and "inclusion aspect ratio" in theoretical inclusion modelling because real pores are not ideal spheroids, while the theoretical model's inclusions are.

To test the electrical-elastic model's performance on the Han data, we first invert equations 18, 19, 22, and 23 for the EPAR associated with each core sample, using the parameters in Table 2 and the measured elastic and electrical data. Rather than solving for a single α which satisfies both bulk and shear modulus measurements in some way, we solve for both the "bulk modulus EPAR", α_K, and "shear modulus EPAR", α_μ, for each sample, by minimising the Root Mean Squared Error (RMSE), which is defined as the square root of the mean of each modelling residual squared. Fournier et al. (2011, 2014, 2018) propose α_K and α_μ are the EPARs which minimise the misfit between the modelled and measured bulk modulus and shear modulus data respectively.

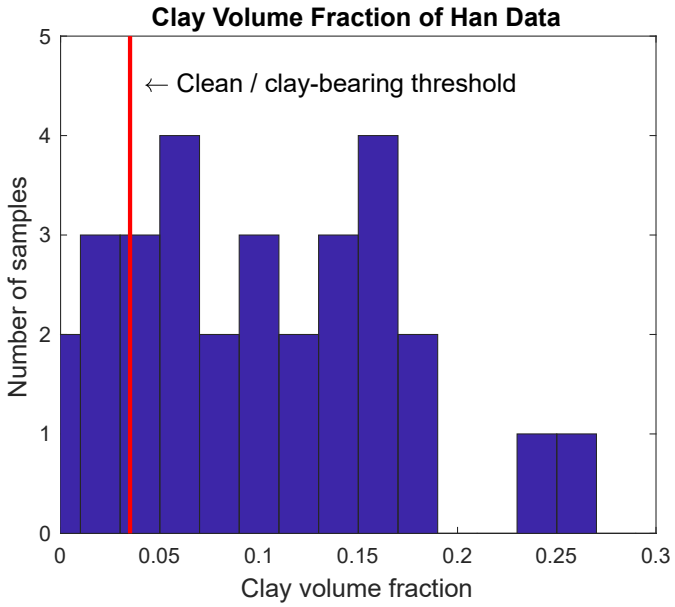

Figure 1. Histogram of the clay content for all samples in the Han data set. The red line at 3.5% clay volume fraction marks the arbitrary cut-off between clean and clay-bearing sandstone samples.

In an ideal composite material with a dilute dispersion of spheroidal inclusions, α_K and α_μ of the medium are expected to be equal (Eshelby 1957). In reality, deviations from the ideal spheroid, or "pore asperities", cause α_K and α_μ to be generally unequal, as observed by Fournier et al. (2011, 2014, 2018) and Cilli & Chapman (2018, 2020).

We display the inverted EPARs, α_K and α_μ, for each sample, with their means, α_{K_0} and α_{μ_0}, and 95% confidence intervals in Figures 2 and 3. We also show inversion statistics in Table 3, including the number of samples in each data subset and the standard deviation of the inverted α_K and α_μ for each data subset. We allow the inversion algorithm to search over the full model space $\alpha \in (0, \infty)$ and, interestingly, find it consistently favours modelling with prolate spheroidal pores, where $\alpha > 1$.

To calculate the optimal model parameters, α_K^* and α_μ^*, we used the average solutions, α_{K_0} and α_{μ_0}, as starting points in non-linear global optimisations which minimised the bulk or shear modulus misfit for all samples. These optimal EPARs are also shown in Table 3. There is a 1.8% difference in α_K^* and a 4.7% difference in α_μ^* between clean and clay-bearing model parametrisations. Thus, we

Table 3. EPAR inversion results for the Han data set and its clean and clay-bearing subsets.

Data set	# Samples	α_{K_0}	α_{μ_0}	*s.d.* (α_{K_0})	*s.d.* (α_{μ_0})	α_K^*	α_μ^*	α_K^*/α_μ^*
All samples	30	17.0	13.0	3.65	1.26	16.4	12.8	1.28
Clean (clay $< 3.5\%$)	6	16.6	12.3	0.78	0.73	16.6	12.3	1.35
Clay-bearing (clay $> 3.5\%$)	24	17.1	13.1	4.07	1.32	16.3	12.9	1.26

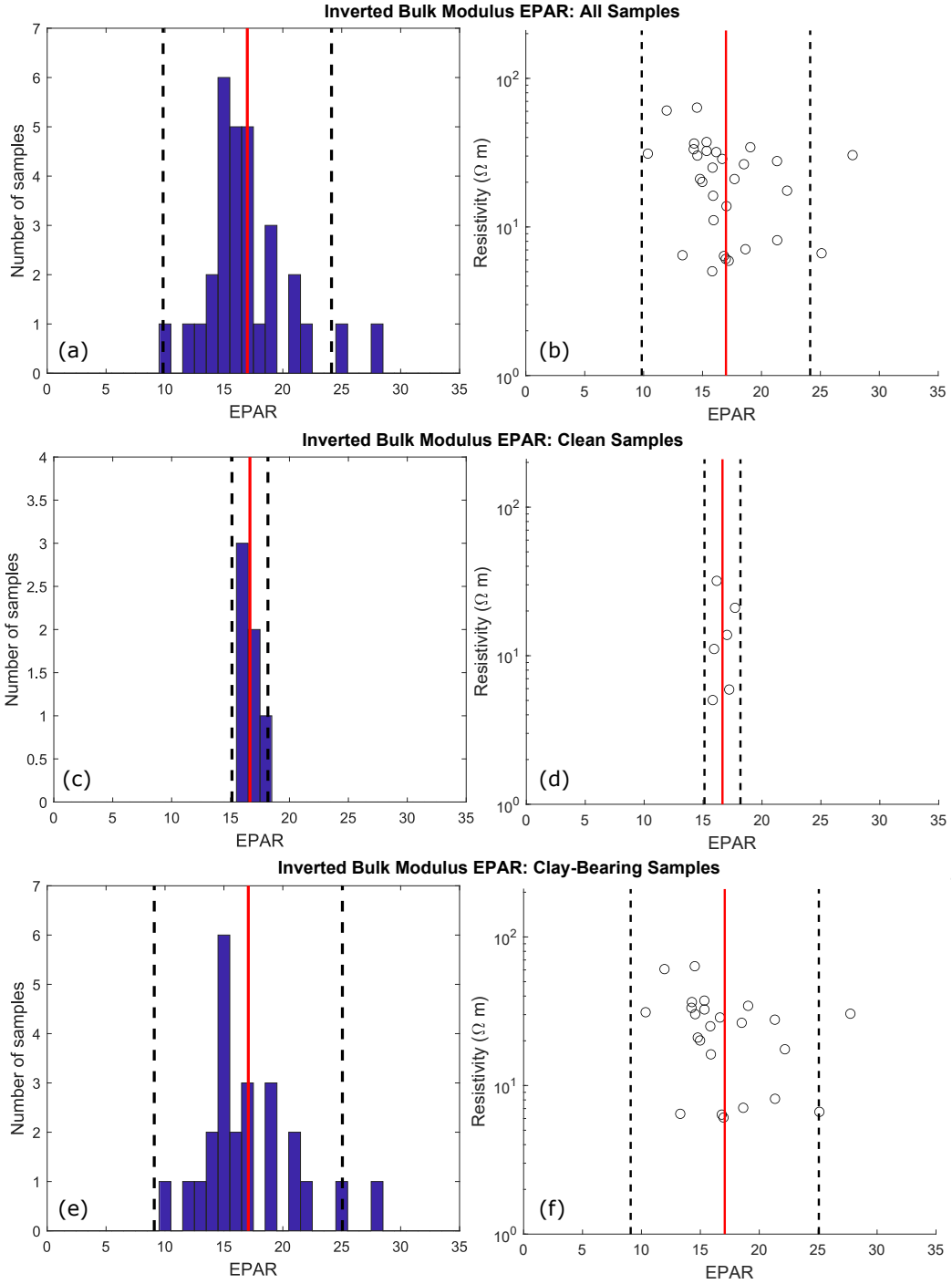

Figure 2. Inverted α_K for each core sample by minimising misfit between measured and modelled bulk modulus. Subfigures a) and b) show all data; c) and d) show clean data; and e) and f) show clay-bearing data. Subfigures a), c), and e) show histograms of inversion results, while subfigures b), d), and f) show the inverted results against measured sample resistivity. The mean EPAR for each data set is shown (red line), as well as the solution's 95% confidence intervals (dashed black).

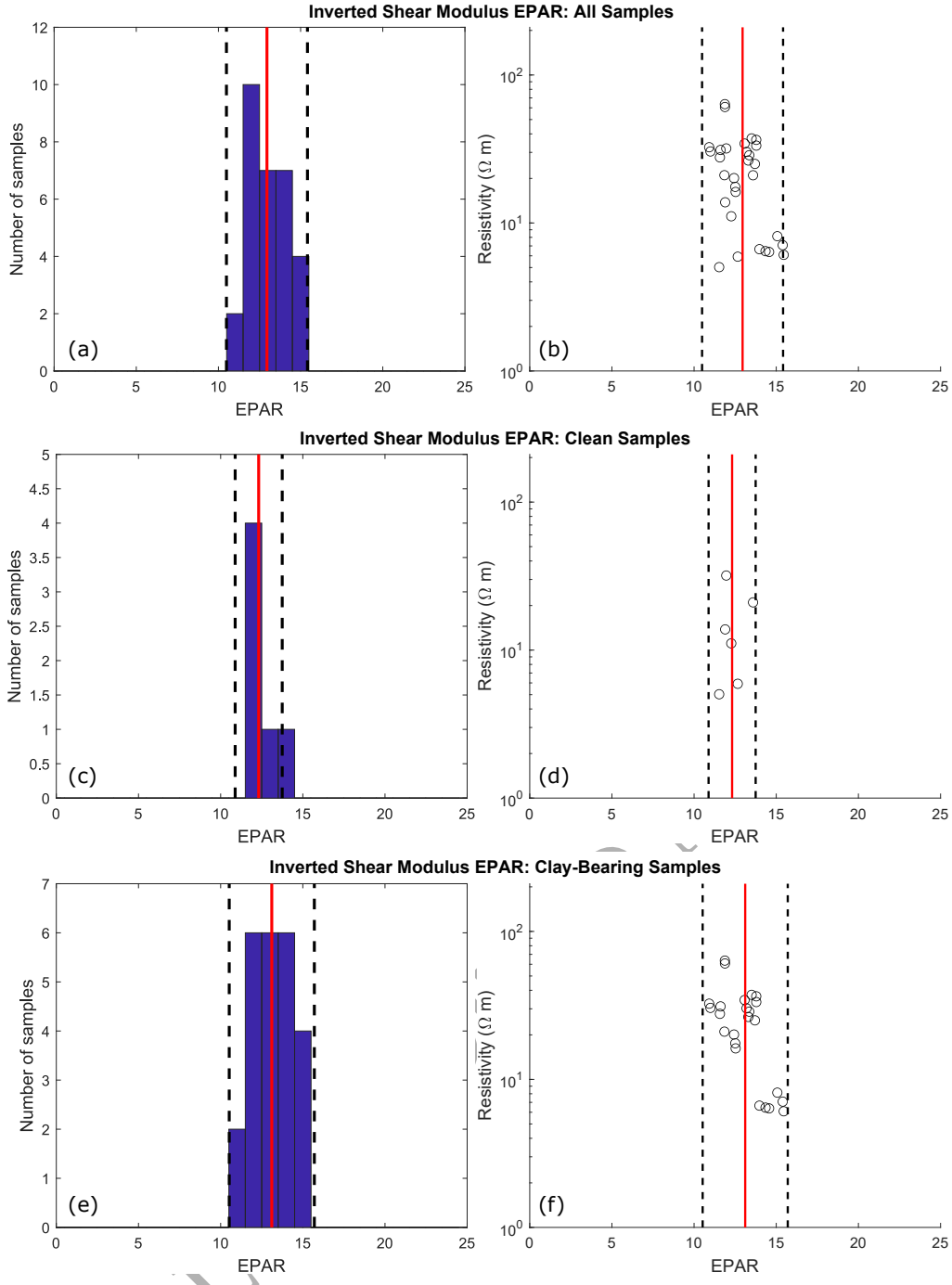

Figure 3. Inverted α_μ for each core sample by minimising misfit between measured and modelled bulk modulus. Subfigures a) and b) show all data; c) and d) show clean data; and e) and f) show clay-bearing data. Subfigures a), c), and e) show histograms of inversion results, while Subfigures b), d), and f) show the inverted results against measured sample resistivity. The mean EPAR for each data set is shown (red line), as well as the solution's 95% confidence intervals (dashed black).

conclude α_K^* and α_μ^* are weakly influenced by clay volume fraction in this data set. The ratio of α_K^* and α_μ^* in this electrical-elastic DEM modelling exercise is also shown in Table 3, and interestingly is not unity, which is an observation previously made only in purely elastic modelling settings.

We forward modelled resistivity-bulk modulus and resistivity-shear modulus trends using α_K^* and α_μ^* respectively, as shown in Figure 4. The propagated 95% confidence intervals from the sample-by-sample EPAR inversions of Figures 2 and 3 are also shown. The joint electrical-elastic Hashin-Shtrikman bounds (Carcione et al. 2007) are displayed, with the proposed electrical-elastic modelling method obeying these bounds in all examples. Being asymptotically correct, the electrical-elastic DEM model converges to the water moduli at 100% porosity and the resistivity of water, and converges to the matrix moduli at zero porosity and the resistivity of matrix material. We note the matrix resistivity is not shown on Figure 4 and so the low-porosity, asymptotic modulus values (red diamonds) do not coincide with the forward modelled trend line in the figure.

3.2 V_p/V_s Modelling

The ratio of a rock's P- and S-wave velocities is of importance in reservoir characterisation as different fluids can have similar shear wave velocities but vastly different compressional velocities. The V_p/V_s ratio of any given rock is also highly sensitive to the rock's porosity due to the often-large differences between pore fluid and mineral velocities. Using the electrical-elastic model presented above, we now predict a rock's V_p/V_s ratio using only electrical measurements, an empirical velocity-density relation, and the model's known parameters, assumed *a priori* to be pre-calibrated.

We consider modelling a V_p/V_s ratio trend through the entire Han data set. The first step is modelling elastic moduli trends (Figures 4a,b) using parameters $\alpha_K^* = 16.4$ and $\alpha_\mu^* = 12.8$ (Table 3). V_p and V_s can then be calculated using the linear elasticity equations and the empirical Gardner (Gardner et al. 1974) relation for sandstones:

$$\rho = 0.31 V_p^{0.25} \,. \tag{24}$$

We use an empirical density-velocity relation here to demonstrate how a V_p/V_s ratio trend can be estimated solely using electrical measurements. However, the use of reliable density measurements, if possible, should lead to more accurate V_p/V_s predictions.

Figure 5 shows a cross-plot of the measured V_p and V_s data, as well as the V_p and V_s trends forward modelled from formation factors spanning some subset of the interval $FF \in]2, 1000[$. Residuals in V_p and V_s have standard deviations of 186 m/s and 151 m/s respectively. The standard deviation of the residuals in V_p/V_s ratio is 0.060. The empirical model for clay-bearing sandstones of Han et al.

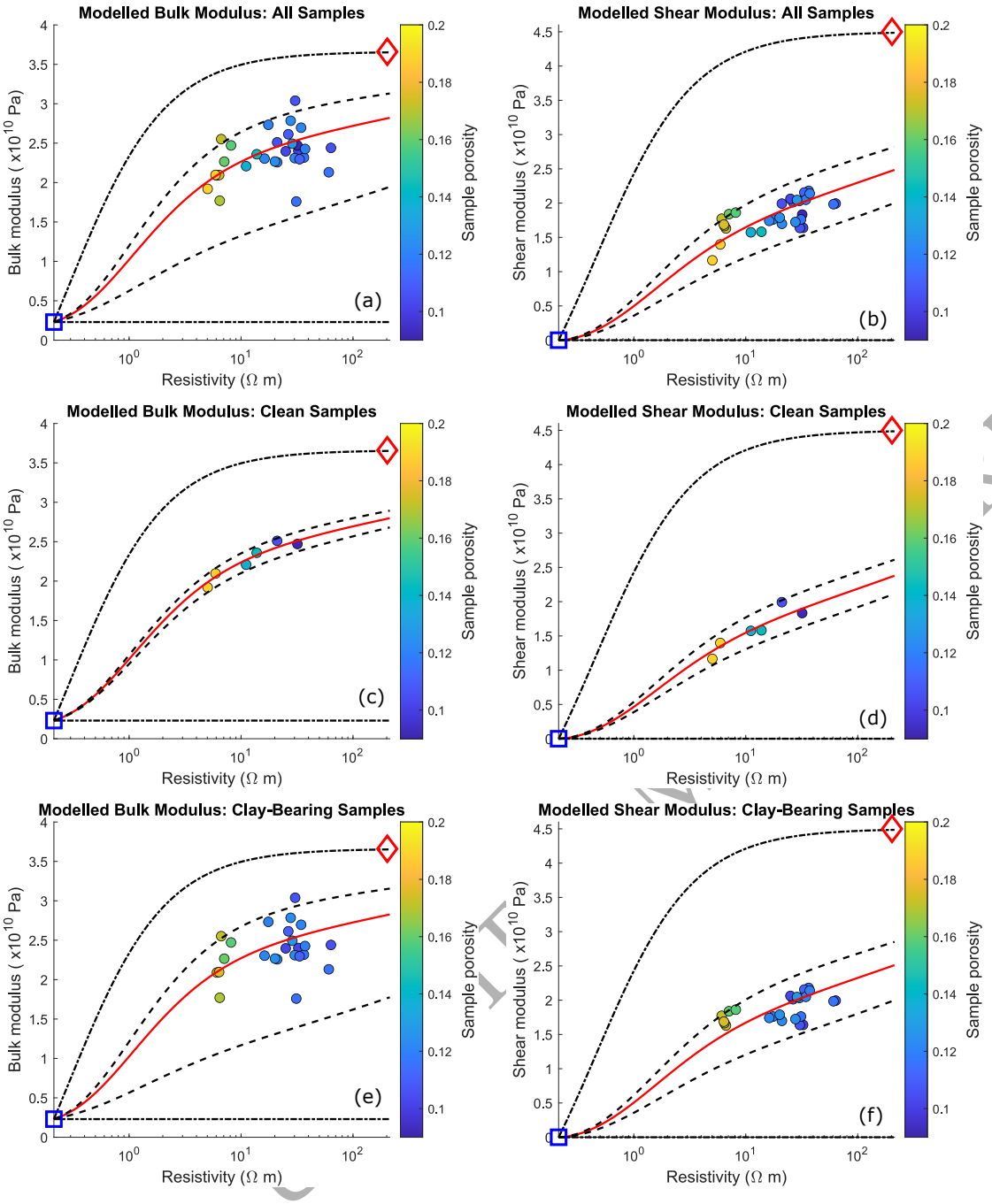

Figure 4. The elastic measurements (circles) of the Han data set and its clean and clay-bearing sample subsets are modelled by solving equations 20 and 21 (red trends) using optimal aspect ratios shown in Table 3. Bulk modulus (left column) and shear modulus (right column) are modelled using parameters α_K^* and α_μ^* respectively. The 95% confidence intervals on initial EPAR estimates, shown in Figures 2 and 3, are forward modelled (dashed curves). The electrical-elastic upper and lower Hashin-Shtrikman bounds are displayed (dot-dashed curves). The electrical-elastic model converges exactly to the properties of water (blue square) at 100% porosity and $\sigma^* = \sigma_2$. It also converges to the properties of matrix material when $\sigma^* = \sigma_1$ and porosity is zero (asymptotic modulus value shown by red diamond). Measured sample porosity (marker colour) is also shown for context.

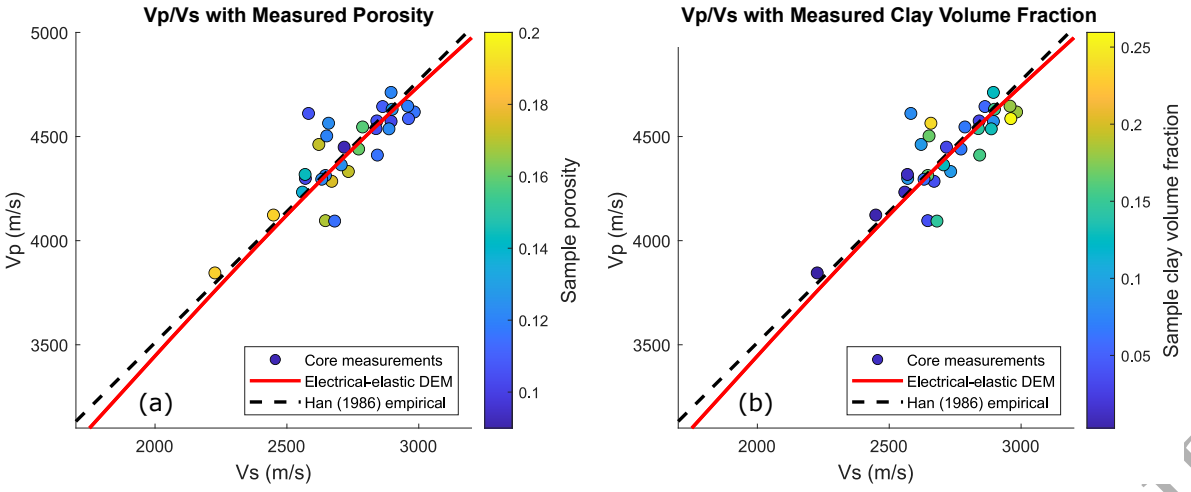

Figure 5. The measured velocities of the Han data set (circles), filled with each sample's a) measured porosity, and b) measured clay volume fraction. The solid red curve shows the V_p/V_s trend predicted by the electrical-elastic DEM model using only resistivity measurements, the empirical Gardner equation, and a prior model calibration. The dashed black line shows the empirical trend of Han et al. (1986) for mixed clay sandstones.

(1986) is shown for comparison. The empirical trend provides a better fit to the data at lower velocities, however it is calibrated on many samples, with shear velocities ranging from less than 1500 m/s to over 3500 m/s. Because of this severe difference in model calibration, we cannot conclude the empirical trend of Han et al. (1986) is actually a better model than the proposed electrical-elastic model.

3.3 Electrical Conductivity Modelling

Having shown a rock's elastic moduli can be modelled from electrical conductivity measurements using cross-property DEM, we now demonstrate a solution to the inverse problem: modelling electrical conductivity from elastic moduli measurements.

We consider the case where a rock's measured bulk and shear moduli are known, as well as the elastic moduli and electrical conductivities of its matrix and pore fluid. We assume α_K and α_μ are known *a priori*. For this example, we also assume *a priori* that α_K and α_μ remain constant in both the forward and inverse mapping of equations 20 and 21. Hence we invert equations 20 and 21 for electrical conductivity using a rock's measured elastic moduli, the known physical properties of the matrix and pore fluid, and a known aspect ratio. As in the case of elastic modelling, we do not require knowledge of the rock's porosity to estimate electrical resistivity from elastic moduli measurements.

Rather than attempting to invert the strongly non-linear coupled differential equations 20 and 21 analytically, we use a numerical approach. Just as we solved for two EPARs, α_K and α_μ, by minimising misfit between modelled and measured bulk and shear modulus respectively, we now

Table 4. Root mean square error (RMSE) for modelling σ_K and σ_μ in the Han data set and its clean and clay-bearing subsets.

Data set	$RMSE(\sigma_K) \times 10^{-2}$ $(1/(\Omega\text{m}))$	$RMSE(\sigma_\mu) \times 10^{-2}$ $(1/(\Omega\text{m}))$
All samples	7.16	4.51
Clean (clay $< 3.5\%$)	1.83	2.77
Clay-bearing (clay $> 3.5\%$)	7.84	4.51

perform two separate inversions for electrical conductivity. One inversion solves for a conductivity, σ_K, by minimising the misfit in measured and modelled bulk modulus using model parameter α_K. The other solves for a conductivity, σ_μ, by minimising the misfit in measured and modelled shear modulus using model parameter α_μ.

Figure 6 demonstrates the inverted resistivities calculated for each subset of the Han data using each sample's experimentally measured bulk and shear modulus, with lines connecting individual inversion results. The 95% confidence intervals on α_K and α_μ are also propagated to resistivities for each sample and connected by dashed lines. Table 4 shows the RMSE for each modelling scenario.

In the presence of clay, the lower scatter in measured resistivity-shear modulus data than in resistivity-bulk modulus data leads to a more accurate (lower RMSE) prediction of sample resistivity through shear modulus inversion than bulk modulus inversion. That is, σ_μ is a more accurate predictor of measured σ than σ_K in the Han data when at least some samples have clay. The modelling of the clay-rich data is less compelling than that of the clean sandstone data. This could be for a range of reasons, including the inappropriate modelling mineralogy and the double layer effect. In the case of clean samples (Fig. 6c and 6d), σ_K is a more accurate prediction of measured σ than σ_μ, however concluding which model is preferable with confidence is hampered by the small number of samples in this data subset.

4 DISCUSSION

Cross-property DEM modelling has a number of advantages over other cross-property models. Namely, the model is theory-based, has no porosity terms, has a single, intuitive model parameter, is correct in the high and low porosity asymptotes, and relates inclusion modelling geometrical functions $P^{(*2)}$, $Q^{(*2)}$, and $R^{(*2)}$. We have shown the model to work on a single data set in this study, however its practical advantage is yet to be seen. A practical advantage may include characterising a rock's physical properties with fewer measurements, for example estimating a rock's bulk and shear modulus in the absence of V_p, V_s, density, and porosity measurements.

The key advantage of the cross-property DEM model is the consistency of the physical assump-

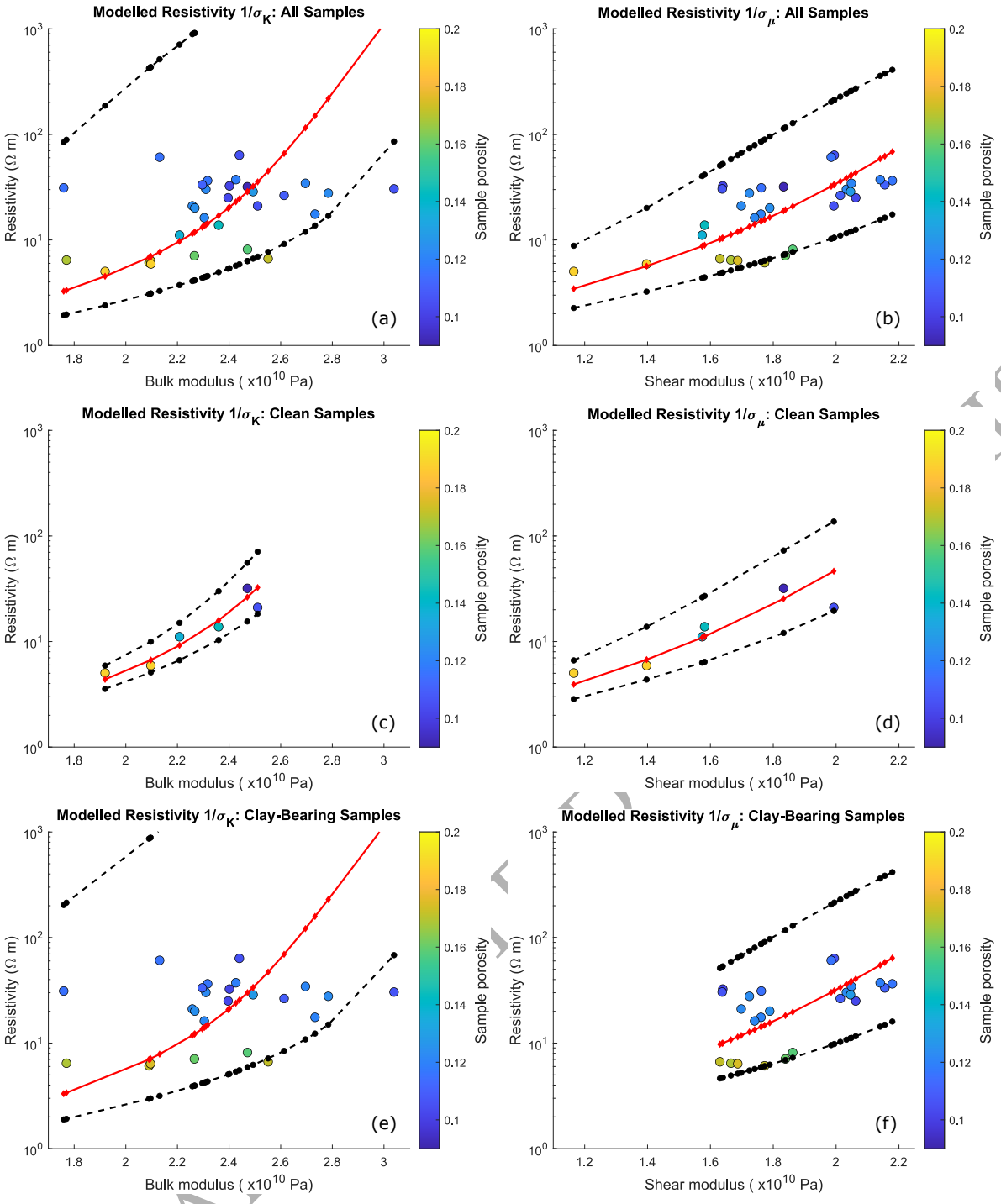

Figure 6. Core measurements (circles) of the Han data set (top row) and its clean (middle row) and clay-bearing (bottom row) sample subsets are modelled by inverting equations 20 and 21 (red diamonds) using optimal aspect ratios shown in Table 3. Resistivities $1/\sigma_K$ (left column) and $1/\sigma_\mu$ (right column) are modelled using parameters α_K^* and α_μ^* respectively. The 95% confidence intervals on initial EPAR estimates are propagated (black points). Measured sample porosity (marker colour) is also shown for context. Lines connect individual inversion results to obviate possible trends.

tions behind the two methods we have combined. In a more empirical approach, this is not necessarily the case.

The proposed electrical-elastic DEM modelling method's preference to approximate pores using prolate spheroids contrasts with typical elastic modelling flows, where pores are often represented by oblate spheroids. Modelling elastic properties with oblate spheroidal inclusions in a DEM framework coincides with the lower Hashin-Shtrikman bound (Norris 1985), while modelling with prolate spheroids does not. This may suggest that prolate spheroids may only be preferable for electrical-elastic modelling so long as the rock's elastic moduli are sufficiently high. We note the data and modelled trends in Figures 4 and 6 all lie within the Hashin-Shtrikman bounds. Additional work on cross-property bounds has been discussed by Gibiansky & Torquato (1996) and Mavko & Saxena (2013).

Figures 2 and 3 show a large scatter in α_K for the clay-bearing data sets. The EPAR parameter in a DEM model is a fitting parameter, absorbing inaccuracies in clay-related parameters, assumptions and the independent variable. The presence of scatter in EPAR when inverted from clay-bearing samples but not clean samples indicates variability in other model parameters or inaccurate assumptions, such as assuming a pure quartz mineralogy or not accounting for the double layer effect.

The scatter in inverted EPARs (Figures 2 and 3) for clay bearing samples is significantly lower in the inversion for α_μ than for α_K. This suggests there is higher modelling uncertainty due to clay content in estimating the effective bulk modulus than shear modulus. This difference in uncertainty is a result of the difference in correlation between measured K and σ, and measured μ and σ, as shown in Figures 4 and 6. In addition to this, Table 3 shows the standard deviation in inverted α_{μ_0} for clean samples and the full data set are very similar. It therefore seems the uncertainty in modelled shear modulus is weakly sensitive to clay content in the Han data.

The presented model accounts for an isotropic stiffness and conductivity, where the electrical and elastic properties are fully described by scalar moduli, rather than electrical resistivity and stiffness tensors. Extending this model to the anisotropic case may be useful, as Singh et al. (2020) showed that elastic EPAR differed depending on the direction of sonic measurement in anisotropic, digital rocks. This anisotropic extension of the model could be of interest as North & Best (2014) showed that even visually isotropic sandstones can have up to 25% anisotropy due to syn-depositional and post-depositional compaction processes.

We present here the basis for a functional form which maps from any of six physical properties (elastic moduli, electrical resistivity, and those in Table 1) to the remaining five properties. The potential application of some of these mappings may not necessarily be in rock physics, where we are predominantly concerned with a rock's elastic and electrical properties. Rather, we expect the appli-

cation of some of these mappings to be in other scientific fields, for example in the engineering or materials sciences.

In the unrealistic scenario of an infinite, isotropic, homogeneous material containing a dilute dispersion of isotropic, homogeneous, randomly oriented ellipsoidal inclusions acted on by a low frequency incident field with its source located at infinity, inclusion modelling theory would suggest a single aspect ratio will predict all properties from all other properties discussed in this paper. We have shown on one data set of clean, wet sandstones that the forward and inverse electrical-elastic cross-property DEM models are both accurate when using a single aspect ratio. However, the disparity between α_K and α_μ in real rocks is seen here and otherwise well documented. This raises the question of whether a single aspect ratio can predict all properties from all other properties in reality.

5 CONCLUSION

By combination of differential effective medium schemes, we derive new relationships between elastic and electrical properties of composite media. The relations are independent of porosity but correct in the high and low porosity limits, depending only on aspect ratio. Fitting this single aspect ratio allows us to accurately model joint elastic and electrical properties of clean sandstones. There is more scatter in the case of clay-bearing rocks but our model identifies the correct trend. We suggest this scatter may be related to a wider range of pore geometries, the double layer effect, or anisotropy of the clay properties. The question of whether this approach can be extended to other cross-property relations remains open.

ACKNOWLEDGMENTS

The authors would like to thank Petrobras and Shell for their sponsorship of the International Centre for Carbonate Reservoirs (ICCR), and for permission to publish this work from the VSP project. We thank Andrew Curtis, Ian Main, Rachel Wood, Anton Ziolkowski, and Giorgos Papageorgiou at the University of Edinburgh, Tongcheng Han at the China University of Petroleum, Qingdao, Angus Best at the UK National Oceanography Centre, Southampton, and Tony Watts at the University of Oxford for their support in this work. We thank Angus Best and Tongcheng Han for providing the experimental data used. We are grateful for the insightful and helpful reviews of this manuscript provided by Dr Dieter Werthmüller and an anonymous reviewer.

Data Availability

The data underlying this article are available in Han et al. (2011b), at https://doi.org/10.1111/j.1365-2478.2010.00940.x.

REFERENCES

Alcocer, J. E., García, M. V., Soto, H. S., Baltar, D., Paramo, V. R., Gabrielsen, P. T., & Roth, F., 2013. Reducing uncertainty by integrating 3D CSEM in the Mexican deep-water exploration workflow, *First Break*, **31**(4), 75–79.

Archie, G. E., 1942. The electrical resistivity log as an aid in determining some reservoir characteristics, *Transactions of the AIME*, **146**(1), 54–62.

Berryman, J. G., 1980. Long-wavelength propagation in composite elastic media II. Ellipsoidal inclusions, *The Journal of the Acoustical Society of America*, **68**(6), 1820–1831.

Berryman, J. G., 1992. Single-scattering approximations for coefficients in Biot's equations of poroelasticity, *The Journal of the Acoustical Society of America*, **91**(2), 551–571.

Berryman, J. G., 1995. Mixture theories for rock properties, *Rock physics and phase relations: A handbook of physical constants*, **3**, 205–228.

Bruggeman, V. D., 1935. Berechnung verschiedener physikalischer Konstanten von heterogenen Substanzen. I. Dielektrizitätskonstanten und Leitfähigkeiten der Mischkörper aus isotropen Substanzen, *Annalen der Physik*, **416**(7), 636–664.

Carcione, J. M., Ursin, B., & Nordskag, J. I., 2007. Cross-property relations between electrical conductivity and the seismic velocity of rocks, *Geophysics*, **72**(5), E193–E204.

Chapman, M., Zatsepin, S. V., & Crampin, S., 2002. Derivation of a microstructural poroelastic model, *Geophysical Journal International*, **151**(2), 427–451.

Chen, J. & Dickens, T. A., 2009. Effects of uncertainty in rock-physics models on reservoir parameter estimation using seismic amplitude variation with angle and controlled-source electromagnetics data, *Geophysical Prospecting*, **57**(1), 61–74.

Choy, T., 2016. *Effective Medium Theory: Principles and Applications*, International Series of Monographs on Physics, Oxford University Press.

Cilli, P. A. & Chapman, M., 2018. Modelling the elastic and electrical properties of rocks with complex pore geometries, in *80th EAGE Conference and Exhibition 2018*, European Association of Geoscientists & Engineers.

Cilli, P. A. & Chapman, M., 2020. The power-law relation between inclusion aspect ratio and porosity: Implications for electrical and elastic modeling, *Journal of Geophysical Research: Solid Earth*, **125**(5), 1–25.

Dvorkin, J. & Nur, A., 1993. Dynamic poroelasticity: A unified model with the squirt and the Biot mechanisms, *Geophysics*, **58**(4), 524–533.

Engelmark, F., 2010. Velocity to resistivity transform via porosity, in *SEG Technical Program Expanded Abstracts 2010*, pp. 2501–2505, Society of Exploration Geophysicists.

Eshelby, J. D., 1957. The determination of the elastic field of an ellipsoidal inclusion, and related problems, *Proceedings of the Royal Society of London A*, **241**(1226), 376–396.

Fournier, F., Léonide, P., Biscarrat, K., Gallois, A., Borgomano, J., & Foubert, A., 2011. Elastic properties of microporous cemented grainstones, *Geophysics*, **76**(6), E211–E226.

Fournier, F., Léonide, P., Kleipool, L., Toullec, R., Reijmer, J. J., Borgomano, J., Klootwijk, T., & Van Der Molen, J., 2014. Pore space evolution and elastic properties of platform carbonates (Urgonian limestone, Barremian–Aptian, SE France), *Sedimentary Geology*, **308**, 1–17.

Fournier, F., Pellerin, M., Villeneuve, Q., Teillet, T., Hong, F., Poli, E., Borgomano, J., Léonide, P., & Hairabian, A., 2018. The equivalent pore aspect ratio as a tool for pore type prediction in carbonate reservoirs, *AAPG Bulletin*, **102**(7), 1343–1377.

Frank, V., 1963. On the penetration of a static homogeneous field in an anisotropic medium into an ellipsoidal inclusion consisting of another anisotropic medium, in *Electromagnetic theory and antennas*, pp. 615–623, ed. Jordan, E. C., The Macmillan Co., New York.

Gardner, G. H. F., Gardner, L. W., & Gregory, A. R., 1974. Formation velocity and density: The diagnostic basics for stratigraphic traps, *Geophysics*, **39**(6), 770–780.

Gibiansky, L. & Torquato, S., 1996. Bounds on the effective moduli of cracked materials, *Journal of the Mechanics and Physics of Solids*, **44**(2), 233–242.

Glover, P. W., 2016. Archie's law - a reappraisal, *Solid Earth*, **7**(4), 1157–1169.

Hamada, G., 2004. Reservoir fluids identification using Vp/Vs ratio?, *Oil & Gas Science and Technology*, **59**(6), 649–654.

Han, D.-h., Nur, A., & Morgan, D., 1986. Effects of porosity and clay content on wave velocities in sandstones, *Geophysics*, **51**(11), 2093–2107.

Han, T., 2018. Joint elastic-electrical properties of artificial porous sandstone with aligned fractures, *Geophysical Research Letters*, **45**(7), 3051–3058.

Han, T., Best, A. I., MacGregor, L. M., Sothcott, J., & Minshull, T. A., 2011a. Joint elastic-electrical effective medium models of reservoir sandstones, *Geophysical Prospecting*, **59**(4), 777–786.

Han, T., Best, A. I., Sothcott, J., & MacGregor, L. M., 2011b. Joint elastic-electrical properties of reservoir sandstones and their relationships with petrophysical parameters, *Geophysical Prospecting*, **59**(3), 518–535.

Han, T., Clennell, M. B., Cheng, A. C. H., & Pervukhina, M., 2016. Are self-consistent models capable of jointly modeling elastic velocity and electrical conductivity of reservoir sandstones?, *Geophysics*, **81**(4), D377–D382.

Han, T., Wei, Z., & Li, F., 2020. How the effective pore and grain shapes are correlated in Berea sandstones: Implications for joint elastic-electrical modeling, *Geophysics*, **85**(3), MR147–MR154.

Hussien, M. N. & Karray, M., 2015. Shear wave velocity as a geotechnical parameter: an overview, *Canadian Geotechnical Journal*, **53**(2), 252–272.

Jensen, E. H., Gelius, L.-J., Johansen, T. A., & Wang, Z., 2013. Consistent joint elastic-electrical differential effective-medium modelling of compacting reservoir sandstones, *Geophysical Prospecting*, **61**(4), 788–802.

Jones, A. G., Fishwick, S., Evans, R. L., Muller, M. R., & Fullea, J., 2013. Velocity-conductivity relations for cratonic lithosphere and their application: Example of southern africa, *Geochemistry, Geophysics, Geosystems*, **14**(4), 806–827.

Kennett, B., Widiyantoro, S., & Van Der Hilst, R., 1998. Joint seismic tomography for bulk sound and shear wave speed in the earth's mantle, *Journal of Geophysical Research: Solid Earth*, **103**(B6), 12469–12493.

Kwon, M. J. & Snieder, R., 2011. Uncertainty analysis for the integration of seismic and controlled source electro-magnetic data, *Geophysical Prospecting*, **59**(4), 609–626.

Mavko, G. & Jizba, D., 1991. Estimating grain-scale fluid effects on velocity dispersion in rocks, *Geophysics*, **56**(12), 1940–1949.

Mavko, G. & Saxena, N., 2013. Embedded-bound method for estimating the change in bulk modulus under either fluid or solid substitution, *Geophysics*, **78**(5), L87–L99.

Mavko, G., Mukerji, T., & Dvorkin, J., 2020. *The rock physics handbook: Tools for seismic analysis of porous media*, Cambridge University Press, 3rd edn.

Maxwell Garnett, J. C., 1904. Colours in metal glasses and in metallic films, in *Proceedings of the Royal Society of London*, vol. 73, pp. 443–445, Royal Society of London.

Mendelson, K. S. & Cohen, M. H., 1982. The effect of grain anisotropy on the electrical properties of sedimentary rocks, *Geophysics*, **47**(2), 257–263.

Norris, A. N., 1985. A differential scheme for the effective moduli of composites, *Mechanics of Materials*, **4**(1), 1–16.

North, L. J. & Best, A. I., 2014. Anomalous electrical resistivity anisotropy in clean reservoir sandstones, *Geophysical Prospecting*, **62**(6), 1315–1326.

Osborn, J. A., 1945. Demagnetizing factors of the general ellipsoid, *Physical Review*, **76**(11-12), 351–357.

Polder, D. & Van Santeen, J., 1946. The effective permeability of mixtures of solids, *Physica*, **12**(5), 257–271.

Salem, H. S. & Chilingarian, G. V., 1999. The cementation factor of Archie's equation for shaly sandstone reservoirs, *Journal of Petroleum Science and Engineering*, **23**(2), 83–93.

Sen, P. N., Scala, C., & Cohen, M. H., 1981. A self-similar model for sedimentary rocks with application to the dielectric constant of fused glass beads, *Geophysics*, **46**(5), 781–795.

Sevostianov, I. & Kachanov, M., 2002. Explicit cross-property correlations for anisotropic two-phase composite materials, *Journal of the Mechanics and Physics of Solids*, **50**(2), 253–282.

Singh, J., Cilli, P., Hosa, A., & Main, I., 2020. Digital rock physics in four dimensions: simulating cementation and its effect on seismic velocity, *Geophysical Journal International*, **222**(3), 1606–1619.

Torquato, S. & Haslach Jr, H., 2002. Random heterogeneous materials: microstructure and macroscopic properties, *Appl. Mech. Rev.*, **55**(4), B62–B63.

Wang, Z. & Gelius, L.-J., 2010. Electric and elastic properties of rock samples: A unified measurement approach, *Petroleum Geoscience*, **16**(2), 171–183.

Waxman, M. H. & Smits, L. J. M., 1968. Electrical conductivities in oil-bearing shaly sands, *Society of Petroleum Engineers Journal*, **8**(02), 107–122.

Werthmüller, D., Ziolkowski, A., & Wright, D., 2013. Background resistivity model from seismic velocities, *Geophysics*, **78**(4), E213–E223.

Yasir, S., Abbas, H., & Jani, J., 2018. Estimation of soil young modulus based on the electrical resistivity imaging (ERI) by using regression equation, in *AIP Conference Proceedings*, vol. 2020, p. 020071, AIP Publishing LLC.